NEONATAL IMAGING

Bronchopulmonary dysplasia from chest radiographs to magnetic resonance imaging and computed tomography: adding value

Nara S. Higano[1,2,3] · Alister J. Bates[1,2,3] · Chamindu C. Gunatilaka[1,2] · Erik B. Hysinger[1,2,3] · Paul J. Critser[4,3] · Russel Hirsch[4,3] · Jason C. Woods[1,2,3,5] · Robert J. Fleck[1,5,6]

Abstract

Bronchopulmonary dysplasia (BPD) is a common long-term complication of preterm birth. The chest radiograph appearance and survivability have evolved since the first description of BPD in 1967 because of improved ventilation and clinical strategies and the introduction of surfactant in the early 1990s. Contemporary imaging care is evolving with the recognition that comorbidities of tracheobronchomalacia and pulmonary hypertension have a great influence on outcomes and can be noninvasively evaluated with CT and MRI techniques, which provide a detailed evaluation of the lungs, trachea and to a lesser degree the heart. However, echocardiography remains the primary modality to evaluate and screen for pulmonary hypertension. This review is intended to highlight the important findings that chest radiograph, CT and MRI can contribute to precision diagnosis, phenotyping and prognosis resulting in optimal management and therapeutics.

Keywords Bronchopulmonary dysplasia · Chronic lung disease of prematurity · Computed tomography · Infants · Lungs · Magnetic resonance imaging · Preterm · Pulmonary hypertension · Radiography · Tracheobronchomalacia

Introduction

Throughout the world there are an estimated 15 million preterm births annually [1]. In the United States, 450,000 babies are born prematurely each year [2], with a 10–12% rate of premature birth. For comparison, most other modern, affluent countries have rates in the 5–8% range. Reduction of preterm birth is a national public health priority. Yet, after years of decline, preterm birth rate has climbed for the last 5 years [2].

Imaging has played a role in the care of preterm births for decades in the form of radiographs, US, fluoroscopy, CT, MRI and to a lesser extent nuclear medicine and angiography. Preterm birth affects all organs, although most of the morbidity and mortality is related to the respiratory system: lungs, airways and pulmonary vascular components. Infants born too early develop infantile respiratory distress syndrome, which is also called surfactant deficiency disorder, and in older literature hyaline membrane disease. Clinical care prioritizes keeping the infants alive so they can continue to grow and mature their organs, but the necessary respiratory support strategies expose the lungs to oxygen, mechanical ventilation pressures, excessive inflation and atelectasis. These traumas and lung development outside the uterus result in aberrant respiratory system development and growth arrest, causing chronic changes called bronchopulmonary dysplasia (BPD) or chronic lung disease of prematurity [3].

Since BPD was first described in 1967, respiratory care has evolved, modes of respiratory support have improved and surfactant therapy has been introduced [4]. This has resulted in improved survival in ever younger and smaller

✉ Robert J. Fleck
robert.fleck@cchmc.org

1 Center for Pulmonary Imaging Research, Cincinnati Children's Hospital Medical Center, Cincinnati, OH, USA

2 Division of Pulmonary Medicine, Cincinnati Children's Hospital Medical Center, Cincinnati, OH, USA

3 Department of Pediatrics, University of Cincinnati College of Medicine, Cincinnati, OH, USA

4 Division of Cardiology, Cincinnati Children's Hospital Medical Center, Cincinnati, OH, USA

5 Department of Radiology, Cincinnati Children's Hospital Medical Center, Cincinnati, OH, USA

6 Department of Radiology, University of Cincinnati College of Medicine, 3333 Burnet Ave., ML 5031, Cincinnati, OH 45229, USA

preterm babies. As a result, the rate of preterm births developing BPD still affects a substantial portion of preterm infants who require respiratory support or have respiratory morbidity after discharge [5].

Portable chest radiograph and chest CT in the evaluation of these children has always been used as a problem-solving tool. However, recent studies have begun to show that CT and MRI of the respiratory system can provide information that is not evident on chest radiograph, thereby providing diagnostic and prognostic information that influences care [6]. Additionally, over the last 20 years, efforts to reduce radiation dose of CT have improved the risk-to-benefit equation [7] and MRI is now becoming a viable method of evaluating the lungs because of ultrashort echo-time (UTE) and other three-dimensional (3-D) high-resolution, proton-density-weighted methods [8, 9]. In this review, we discuss the literature and present information that radiologists can use in evaluating the respiratory system in preterm infants in the post-surfactant era with chest radiograph, and the added value of CT and MRI.

Bronchopulmonary dysplasia, defined

A persistent challenge in the study and treatment of BPD is the lack of an effective definition, in part because of the multifactorial mechanisms of this unique disease. BPD was first described by Northway et al. [10] based on radiographic (Fig. 1) and pathological evidence of pulmonary disease (opacification, atelectasis, cysts, lucencies). While varying definitions have been proposed since then, they remain mostly operational, relying on degree and duration of oxygen requirement rather than pathophysiological condition [11].

In 1988, Shennan et al. [12] followed 600 preterm infants with birth weights <1,500 g for 2 years and determined that an oxygen requirement at 36 weeks post-menstrual age (PMA) was predictive of abnormal pulmonary function in the first 2 years after birth. However, there was increasing recognition through the 1990s that improvements in antenatal and postnatal treatment strategies were changing the pathophysiology of BPD (so-called new BPD) — namely, very-low-birth-weight infants with seemingly mild lung disease in early neonatal life were developing increasing ventilatory needs and undergoing pronounced alveolar and vascular "growth arrest" [13]. In response, a new diagnostic definition was proposed at a workshop in 2000 sponsored by the National Institutes of Health (NIH) National Heart, Lung and Blood Institute (NHLBI) and published in 2001 [13]. This 2001 consensus definition included graded severity levels based on gestational age and level of required respiratory support. Specifically, infants diagnosed with BPD require oxygen therapy for at least 28 cumulative days, with mild, moderate and

Fig. 1 Typical appearance of bronchopulmonary dysplasia (BPD). Anteroposterior (AP) chest radiograph of a girl born at 25 weeks of gestation who is now post-menstrual age 36 weeks (11 weeks old) with severe BPD. The girl is still intubated and has a ductus arteriosus closure device. The lungs are characterized by overall hyperinflation, with mixed areas of density and hyperlucency characteristic of the AP chest radiograph appearance of severe BPD

severe grades determined by degree of respiratory support required at 36 weeks of post-menstrual age; while initially helpful in delineating severity, many infants eventually became unclassifiable with updated clinical practices such as high-flow nasal cannula with 21% oxygen or low-flow with 100% oxygen. Although additional clinical definitions have attempted to improve upon this definition (e.g., a physiological challenge of supplemental oxygen withdrawal) [14–16], the 2001 consensus definition has been implemented most widely, despite the inconsistent relationship between various BPD definitions and clinical outcomes [17–19].

A new definition was proposed in 2018 at a conference conducted by the NIH Eunice Kennedy Shriver National Institute of Child Health and Human Development (NICHD) to incorporate newer modes of noninvasive ventilation and address several deficiencies, including institutional variability, lack of evidence-based guidelines, and unclassified status of prematurity-related deaths prior to 36 weeks of post-menstrual age [3]. This 2018 definition asserts that a premature infants (<32 weeks of gestational age) with BPD have persistent parenchymal disease and use respiratory support at 36 weeks of post-menstrual age (grades I, II or III based on fraction of inspired oxygen [FiO2] range/oxygen level/oxygen concentration). Importantly, this refined BPD grading system reincorporated radiographic confirmation of parenchymal lung disease. Like previous definitions, this 2018 workshop definition struggles with early identification of infants who will eventually have severe chronic lung disease of prematurity; imaging performed early in the neonatal

intensive care unit (NICU) might allow clinicians to apply targeted therapies to the most at-risk infants.

Chest radiograph

Chest radiograph has always been at the forefront of decision-making in infants with respiratory distress. Northway et al. [10] first reported four stages of chest radiograph findings that can occur in preterm infants and coined the term BPD. By today's standards the preterm infants were relatively large and at relatively advanced gestational ages. Since that time, treatment of mothers at risk of preterm birth and infants born preterm has evolved greatly and continues to evolve, as does the appearance of the chest radiograph.

The use of chest radiographs in infants for problem-solving is well established. However, over the years chest radiography has been proposed as part of the BPD definition and used to predict clinical outcomes such as growth, respiratory distress and gas exchange [20, 21]. In 1984, Toce et al. [21] developed a scoring system that included lung expansion, interstitial densities, focal emphysema (cysts) and cardiovascular abnormalities. Interestingly, they suggested that 2 weeks after birth is the most specific time to diagnose BPD [21]. Several authors in the 1980s noted that the evolution of chest radiography was nonlinear and appeared to be resulting from the changing treatments, including use of antenatal steroids in mothers, changing ventilation strategies and postnatal steroid treatments.

However, the most major change was noted when exogenous surfactant became clinically available in the early 1990s [22, 23], as described by Swischuk et al. [24]. The first radiograph demonstrated the granular appearance typically associated with preterm birth and surfactant deficiency, and 76% of infants cleared the granular opacities by 1 day old (Fig. 2). Subsequently, 45% remained clear and did well, but these also tended to be the larger infants

with a more mature gestational age. The remaining 55% of infants developed hazy to opaque density in the lungs (Fig. 2) by the second week after birth, termed "leaky lung syndrome." Only 11% of these became clear again. Lungs that did not clear went on to develop the cystic bubbly lucencies that are now typically associated with BPD (Fig. 1) [24].

Chest radiography studies looking at future growth noted that hyperinflation worsened along with focal areas of emphysema and interstitial opacities at 1 year compared to 1 month [25–27]. Moya et al. [28] investigated the ability of the chest radiograph obtained at 36 weeks of postmenstrual age to predict BPD by using a grading system and found that low scores were less reliable in predicting BPD outcome, but prediction improved with increasing scores. Kim et al. [29] found that an interstitial or coarse interstitial pattern (Fig. 2) at day 7 after birth was predictive of BPD developing with high specificity but low sensitivity, but that birth weight, gestational age and invasive ventilation were much more sensitive. More recent studies have related the cystic bubbly changes to a higher need for oxygen therapy [30], and a large study by Arai et al. [31] with a cohort of more than 8,000 infants showed that bubbly/cystic changes at 28 days was more predictive of home oxygen therapy than gestational age, birth weight, chorioamnionitis or any other factor. Those without the bubbly/cystic changes had only 2% rate of home oxygen. Bubbly/cystic change is also associated with wheezing [32, 33].

In sum, the chest radiograph of preterm infants starts with a granular pattern on day 1, often clears with administration of surfactant and then a substantial number of preterm infants develop diffuse opacity in the second week. As that diffuse opacity evolves into an interstitial, coarse or bubbly pattern, it becomes more predictive of BPD and outcomes after hospitalization. Although the coarse, interstitial bubbly pattern is specific, it lacks sensitivity.

Fig. 2 Evolving lung appearance on radiography in a premature newborn. **a** Anteroposterior (AP) chest radiograph in a 1-day-old boy born at 24 weeks of gestation shows diffuse, fine granular opacities throughout the lungs, often with air bronchograms. **b** AP chest radiograph of the same boy at 2 days old. Surfactant had been adminis-tered and the boy was extubated. At this time the lungs appear clear and better inflated. **c** AP chest radiograph in the same boy at 4 days of age shows that his lungs have become much more opaque and coarse, with mixed lucent and opaque areas resulting in reintubation

Computed tomography

The role of chest CT in preterm infants during their period of neonatal intensive care is largely based in problem-solving for more complex cases (and the same is true later in life), but numerous studies have evaluated the lung parenchyma and related the findings to severity of BPD or outcomes. These studies are split between early life and later life. The lung findings of BPD on CT are a recapitulation of those on chest radiograph, but with greater detail and richness (Fig. 3). Several studies laid the groundwork for CT scoring [34–38]. We focus here on the more recent CT studies because they reflect the current post-surfactant era of care.

The common thread among all of these CT studies was the objective findings on either high-resolution CT or chest CT. Researchers brought these all together in a relatively simple scoring system that related the score to the severity of BPD and, to a lesser degree, outcome [39, 40]. Hyper-aeration of the lung, including global and focal air-trapping and mosaic perfusion, has been a common theme of all of these studies [34–40] and continues to be a primary theme [41–51]. A second category is "emphysema," which Ochiai et al. [40] described as a sharply demarcated area of low attenuation. However, later-in-life reports of "emphysema" are variable as to the presence of this finding and description [37, 38]. There is also speculation that the emphysema identified in older children and young adults might be progressive [47, 48], but there is not proof of this. The third category is structural change, which includes linear opacities, triangular subpleural opacities and atelectasis/consolidative opacities [40, 47].

There is a substantial difference between the appearance of the lungs early in life [5, 40, 41, 49] when the infants first become stable enough for imaging, and later in life when the lungs have had time to heal and further develop. In general, the size and number of pulmonary opacities decrease as the child matures [49]. Simpson et al. [48] reported bronchial wall thickening and exposure to tobacco smoke as the most significant predictors of pulmonary functional decline in school-age children with a history of preterm birth, hypothesizing that the thickening reflected more inflammation or bronchial reactivity.

Dynamic-volume CT or cine CT is a method of using CT to look at the lung over a short period of time using a very low dose for each rotation of the CT to collect imaging data. The advantage is that this type of CT can show changes in the lungs and large airway over a respiratory cycle [52, 53]. This has been described as a method for choosing positive end-expiratory pressure in children with BPD and tracheobronchomalacia [52], which is a critical component related to preterm morbidity [53] and can also be used to evaluate regional lung ventilation [54].

The use of CT early in BPD is most limited by transportation of unstable infants to the CT scanner and to a lesser extent by concern about radiation. However, the association of CT findings to clinical course, pulmonary function and disease progression suggests that CT could play an increasing role in evaluating preterm babies that goes beyond problem-solving. A non-contrast chest CT performed at discharge from the NICU with a non-sedated feed-and-swaddle technique has the potential to provide information that would identify suspected findings, predict the early clinical course, and potentially decrease hospitalization in the first year after birth [8, 55].
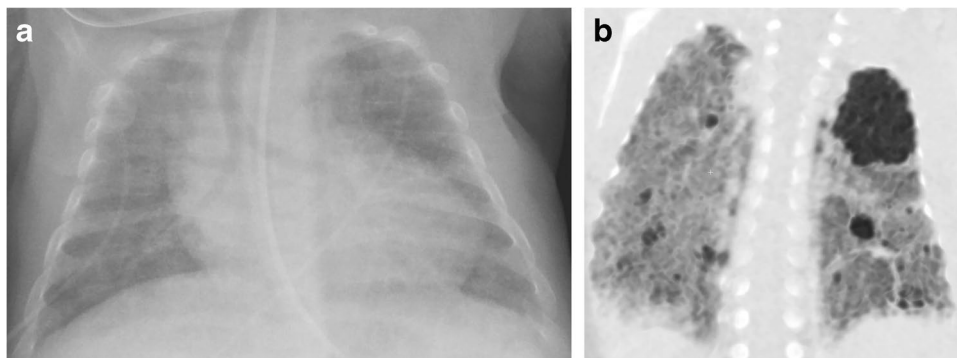

Fig. 3 Lung findings of bronchopulmonary dysplasia on radiography and CT. **a** Anteroposterior (AP) chest radiograph of a premature infant girl born at 23 weeks of gestation, now post-menstrual age 38 weeks (15 weeks old). Portable chest radiograph shows diffuse increased density throughout the lungs but no evidence of air-trapping or cystic changes. **b** Coronal oblique minimum-intensity projection reconstructed CT image demonstrates hyperlucent lung in the left upper lobe and small cysts throughout the lungs. CT also suggested tracheomalacia was present (not shown)

Chest magnetic resonance imaging

In recent years, chest MRI in preterm infants has been implemented to provide clinically meaningful information using readily available sequences, such as a fast gradient echo (GRE) and spin echo, that can evaluate lung tissue in infants with lung disease without requiring ionizing radiation [56, 57]. Walkup et al. [56] showed that GRE images demonstrate a significantly greater volume of high-intensity lung (putatively combinations of fibrosis, edema, consolidation and atelectasis) in infants with BPD compared with full-term infants and preterm infants who were not diagnosed with BPD. However, the volume of low-intensity lung did not discriminate clinical BPD diagnoses, despite the established presence of low-density lung pathologies in BPD such as alveolar simplification, cysts, emphysema and air-trapping. This is likely attributable to that fact that conventional Cartesian sequences typically cannot achieve minimum echo times (TE) below the lung parenchymal $T2^*$ (~ 0.5–3 ms at typical field strengths) and thus do not provide sufficient image contrast between short-$T2^*$ tissues and true cystic/air-trapped regions [58]. Even so, radiologic reader scores from a modified Ochiai system that evaluates parenchymal abnormalities (discussed in detail later) [40] significantly delineated all three groups of preterm infants with BPD, preterm infants without BPD, and term infants.

Recent technical developments in sequence acquisition have opened the door to pulmonary MRI using center-out 3-D k-space acquisitions with ultrashort echo times (UTE) and zero echo times (ZTE) [9, 59–63]. Unlike Cartesian sequences, these center-out sequences are inherently robust to subject motion, reducing the need for sedation/anesthesia. Further, these short-TE acquisitions have strong proton-density weighting, allowing for more accurate visualization and quantification of both hyper- and hypodense lung parenchymal tissue. Nozawa et al. [64] demonstrated the potential for ZTE MRI (pointwise encoding time reduction with radial acquisition, or PETRA) to acquire CT-like proton-density-weighted pulmonary images in two infants with congenital cystic lung disease, which is likely to be similarly effective when implemented in infants with lung disease of prematurity. Further, our Center for Pulmonary Imaging Research at Cincinnati Children's Hospital has demonstrated that regional lung intensity on UTE MRI is quantitatively comparable to lung density on chest CT (Fig. 4) in individual neonates with lung disease who underwent both MRI and CT [65]. Using this UTE MRI method, Higano et al. [65] examined whole-lung density distributions in 38 infants with and without BPD and found that the percentage of lung volume with abnormally hyperdense and hypodense tissue

density (defined as $> +1\sigma$ or $< -1\sigma$, respectively, compared to an average control distribution) correlated moderately with clinical BPD severity diagnosis ($R^2 = 0.21$) but more strongly with respiratory support at discharge from the NICU ($R^2 = 0.45$). In an additional study, Higano et al. [66] showed that modified Ochiai scoring of paired UTE and GRE lung images from neonates with BPD (Fig. 5) correlated with duration of various respiratory support levels more strongly than any individual clinical measure (ventilator support, $R^2 = 0.86$; positive pressure ventilation, $R^2 = 0.91$; any support, $R^2 = 0.77$).

As MRI strategies emerge to evaluate neonatal lung structure, so, too, do complementary MRI strategies for measuring lung function. UTE MRI sequences inherently acquire the center of k-space (k_0) at every acquisition, which can be exploited as a self-navigating signal for respiratory gating (Fig. 6) that allows raw data to be binned and selectively reconstructed at different phases of the respiratory cycle [67–71], often from a child who was scanned during tidal breathing. Advanced reconstruction strategies, such as iMoCo (iterative motion-compensation reconstruction) UTE MRI, have demonstrated high-scanning efficiency, sharper anatomical lung structures and higher apparent signal-to-noise ratio compared to other motion-correction methods in free-breathing pulmonary MRI of adults and pediatrics. Zhu et al. [72] showed the feasibility of neonatal iMoCo UTE in one non-sedated 10-week-old with pulmonary interstitial glycogenosis, demonstrating the ability to capture and reject non-compliant bulk motion. Using dynamic images throughout the breathing cycle, various respiratory metrics of interest have been measured in neonates with lung disease, including tidal volume, hyperexpansion, global minute ventilation, degree of central airway collapse and tracheal work of breathing [69, 73–76]. By measuring local changes in signal intensities or anatomical deformation throughout the breathing cycle, dynamic pulmonary MRI strategies also open the door to quantitative lung ventilation, similar to techniques used with chest CT [77], but during free-breathing and without ionizing radiation. Capaldi et al. [78] recently implemented convolutional neural networks in deep learning to generate synthetic ventilation images from free-breathing pulmonary MRI in adults with various lung diseases, with a correlation between ventilation defect percentage from MRI and forced expiratory volume in 1 s (FEV_1) from spirometry ($P < 0.001$); similar strategies might be readily translatable to evaluating pulmonary function in the neonatal population.

While tidal-breathing ^{1}H chest MRI strategies are emerging to indirectly measure regional ventilation, hyperpolarized inhaled noble-gas (^{3}He and ^{129}Xe) MRI has been used for several years as a more direct ventilation metric, with established safety [79–81] and numerous applications in a variety of adult and pediatric lung disorders [82–84]. Altes

Fig. 4 Comparison of five
neonates' matched axial CT and
axial ultrafast echo-time (UTE)
MRI slices obtained at a similar
time visually demonstrates
the similarity of tissue density
and lung findings. Subject A is
a neonate with severe bron-
chopulmonary dysplasia (BPD).
The quantitative density of UTE
is highly correlated with CT
density in the lung. Note the dif-
ferent appearance in the spinal
canal on the MRI caused by the
different T1 and T2* properties
in the spinal canal compared
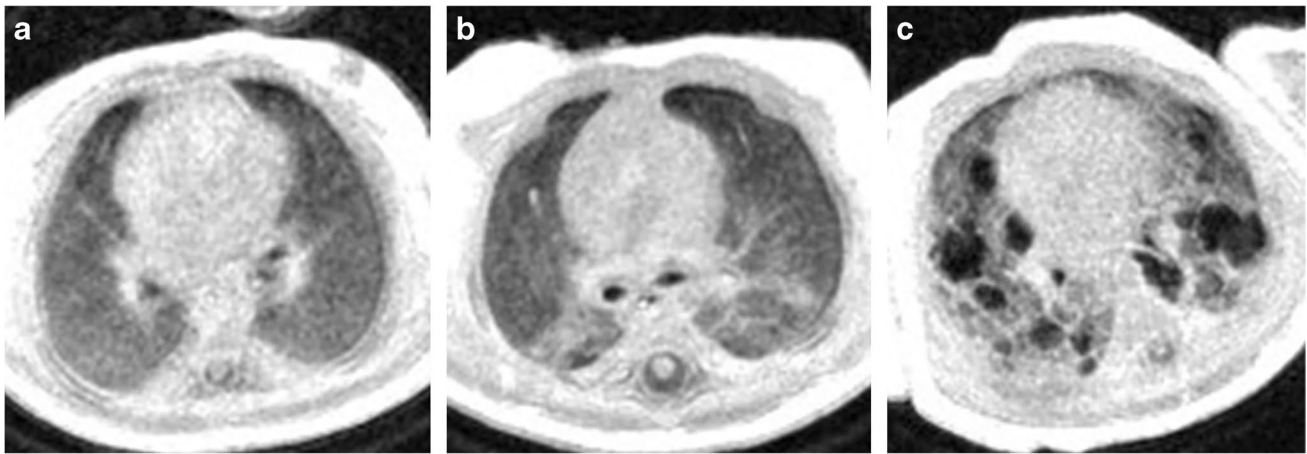to the lung tissue. Reproduced
with permission [64]
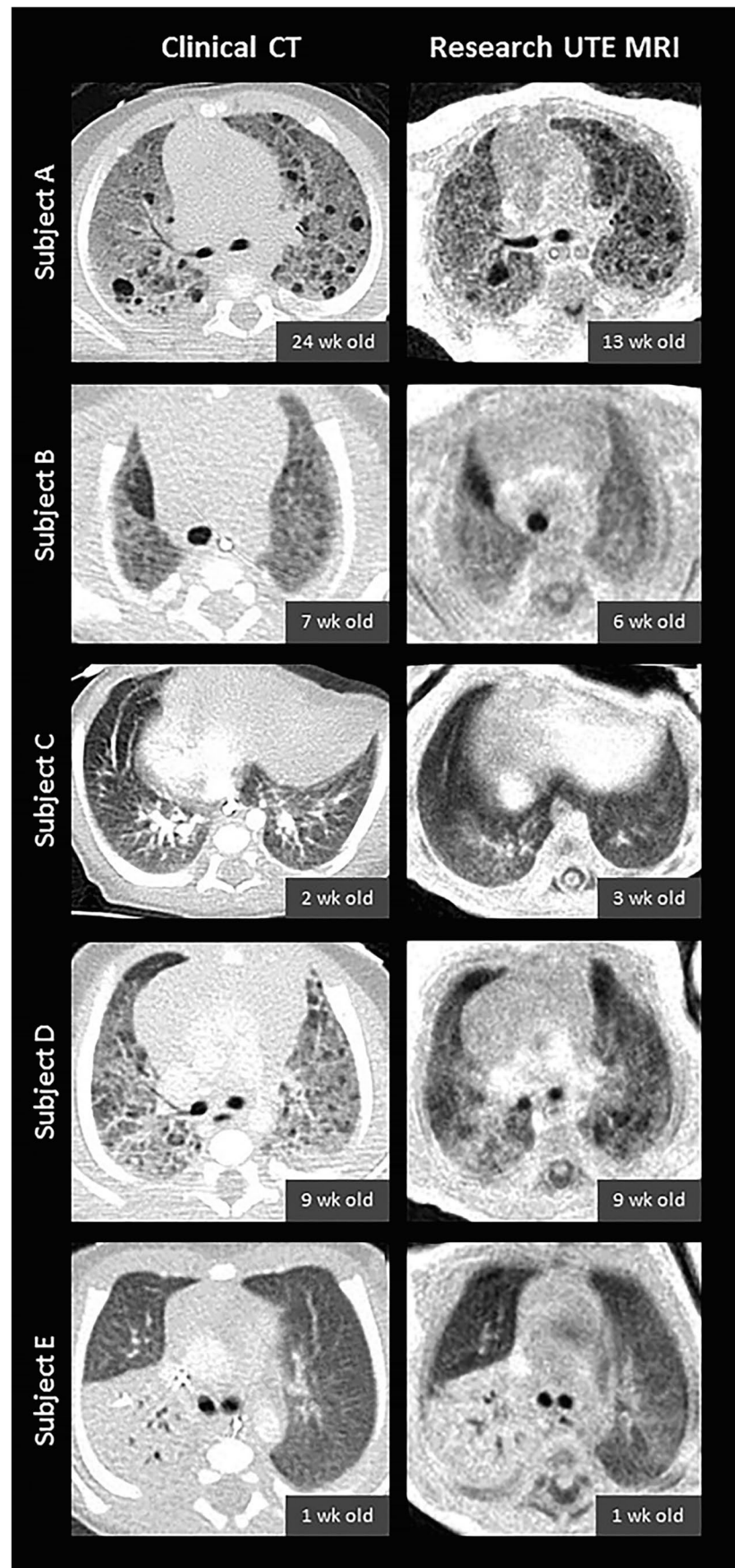
Fig. 5 Axial ultrashort echo-time (UTE) MRI and modified Ochiai score. **a–c** Examples of preterm female born at 26 weeks of gestation, now post-menstrual age 38 weeks (12 weeks old) with mild (**a**), preterm female born at 25 weeks of gestation, now post-menstrual age 41 weeks (16 weeks old) with moderate (**b**) and preterm male born at 23 weeks of gestation, now post-menstrual age 40 weeks (17 weeks old) with severe (**c**) bronchopulmonary dysplasia on axial UTE MR images of the lung based on the modified Ochiai score. The mild patient (**a**) was scored as 1 out of 14, the moderate patient (**b**) 6 out of 14 and the severe patient (**c**) 12 out of 14. Increasing score was positively correlated with greater need for respiratory support and short-term clinical outcomes

et al. [85] recently developed a gas ventilation imaging protocol for MRI acquisition sequences and gas-delivery strategies in a proof-of-concept study with seven non-sedated children younger than 4 years, including one healthy infant, three infants with cystic fibrosis, and one infant born prematurely at 28 weeks of gestation; in this small feasibility study, focal ventilation defects were clearly identified in children with respiratory disease. Hyperpolarized gas MRI can also probe the length-scales of microstructural alveolar airspaces by detecting Brownian airspace diffusion of inhaled gas particles [86]. This technique has been implemented in older pediatric survivors of preterm birth [87] and in an explanted neonatal lung specimen with filamin-A mutation (closely representing BPD lung disease) [88], with significantly elevated apparent diffusion coefficient (ADC) values in children with disease compared to age-matched controls demonstrating enlarged gas-exchange units. While not yet implemented in live neonates, inhaled gas diffusion MRI has strong potential to elucidate abnormal and interrupted alveolar development in infants born preterm.

Trachea and large airways

In addition to the arrest in development of the pulmonary parenchyma, neonates who are born prematurely have disruption in development of the central airway. The net impact of preterm birth is that the central airway is smaller, more compliant and more susceptible to airway injury, especially in neonates who require endotracheal intubation and positive pressure ventilation [89–92]. Consequently, disease of the central airway is quite common in neonates with BPD.

Central airway disease can be divided into dynamic and fixed central airway pathology and results in increased respiratory morbidity in these fragile infants.

Dynamic airway lesions such as tracheobronchomalacia are identified in 10–48% of neonates with BPD undergoing bronchoscopy, which is the reference standard for diagnosis [53, 75, 93, 94]. However, the true prevalence is unclear because children undergoing bronchoscopy are a heavily biased subset, and many neonates who do not undergo bronchoscopy have dynamic airway collapse (Fig. 7) based on advanced imaging techniques [74]. Tracheobronchomalacia is associated with increased morbidity during the initial hospital admission with prolonged need for mechanical ventilation, longer hospitalization and increased need for tracheotomy [53]. Following discharge, children with tracheobronchomalacia require more medical therapies and feeding support [53] and have increased frequency of rehospitalization, particularly during respiratory illnesses [95].

Fixed airway lesions such as subglottic stenosis are also common in those neonates who require invasive mechanical ventilation. The cricoid is the narrowest portion of the airway and is particularly susceptible to injury from intubation in neonates. The prevalence of post-intubation subglottic stenosis in neonates is 0.9–8.3% [96] and is likely higher in those with BPD than the general neonatal population because of the small airway size, need for prolonged intubation, and multiple intubation attempts [97]. As with tracheobronchomalacia subglottic stenosis is diagnosed by bronchoscopy and utilizes the Myer-Cotton scale (Fig. 8), which grades severity based on the largest endotracheal tube that permits an air leak at 20 cm H_2O [98]. Depending on the severity of subglottic stenosis, treatment options range from observation or endoscopic

Fig. 6 Preterm female born at 27 weeks of gestation, now post-menstrual age 36 weeks (9 weeks old). Self-navigating signal obtained from the center of ultrashort echo-time (UTE) MRI k-space (k_0). **a** Graph illustrates the difference in the signal between the signal obtained in quiescent tidal breathing (*multi-colored line*) and when the child is moving significantly (*dark blue*). This allows data from bulk motion to be discarded. **b** Graph is a magnification of a smoothed and binned signal of the quiescent tidal-breathing signal. The colors of the segments in the line correspond to the phases of respiration. Blue is end-expiration and dark maroon is end-inspiration. **c** Each respiratory bin can then be reconstructed into an image during a different phase of respiration, which is shown in the line of coronal UTE MRI lung images. The movement of the diaphram and chest wall, and the change in lung density, is illustrated. This has been shown to have potential for regional ventilation maps
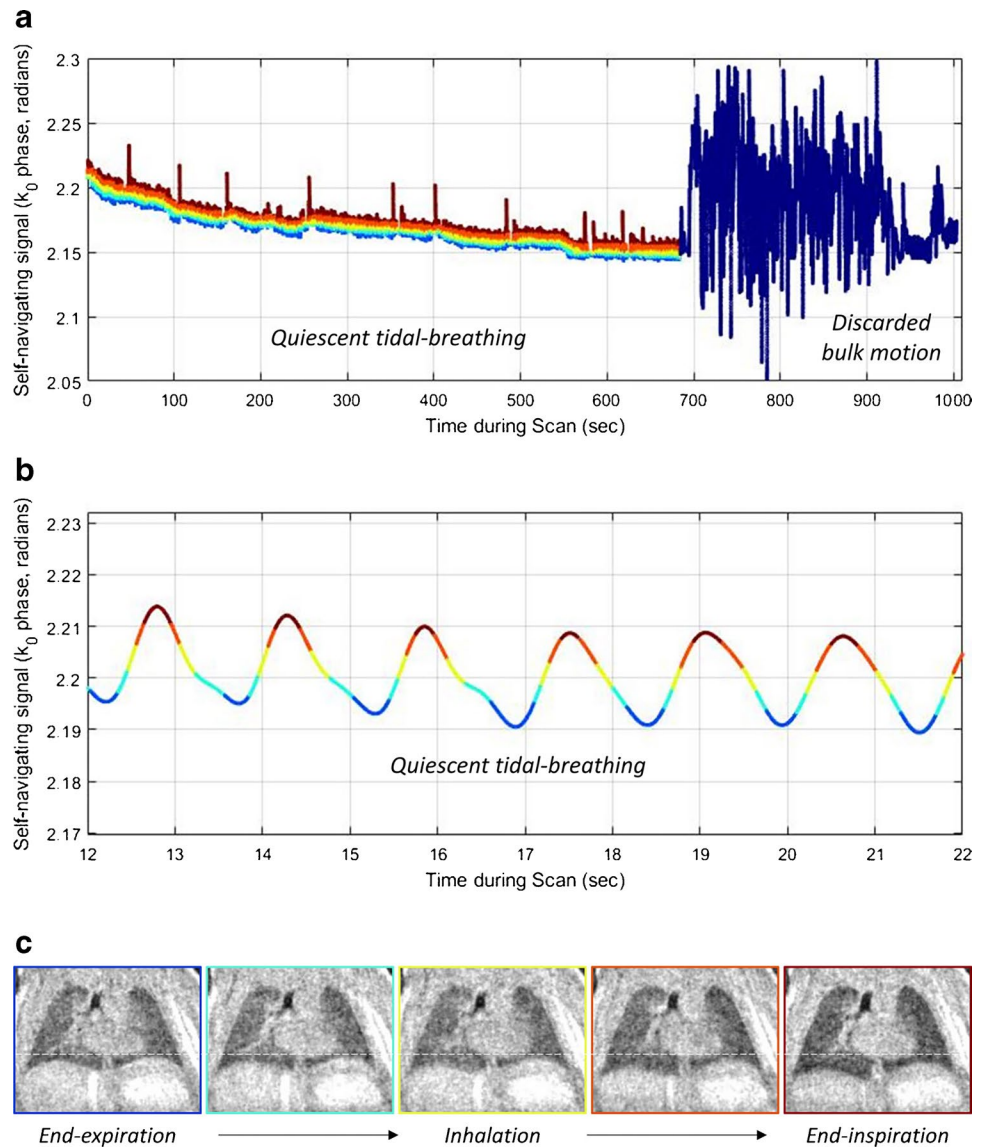
balloon dilation for milder stenosis to open airway surgery or tracheotomy for more severe disease [99, 100].

Despite the impact of central airway disease on children with BPD, our understanding is limited because the diagnosis typically relies on direct visualization with bronchoscopy. However, recent advances in imaging technologies such as CT and MR can provide a noninvasive way to assess the neonatal airway without sedation. In the case of MR, this can be done without ionizing radiation and thus might be suitable for longitudinal population studies of central airway disease in BPD.

Central airway magnetic resonance imaging

Magnetic resonance imaging has been used to noninvasively investigate airway abnormalities such as tracheo-bronchomalacia and subglottic stenosis in neonates and

animal models of neonates [101–103]. Retrospective respiratory gating of UTE MRI, the same sequence that evaluates the lung parenchyma, simultaneously allows measurement of 3-D dynamic changes in lumen size [74]. Assessing the cross-sectional area of the tracheal lumen based on UTE MRI (Fig. 9) has been shown to diagnose tracheomalacia with equivalent accuracy to bronchoscopy [75].

Until recently, MRI has only been used to depict anatomy and the significance of the tracheomalacia has been inferred, but tracheomalacia likely has a profound effect on energy needs of these tiny preterm babies. Using MRI as a technique for imaging airway anatomy and motion, computational fluid dynamics can calculate airflow parameters such as airway resistance or pressure gradients based on airway anatomy, motion and MRI-derived tidal volumes (Fig. 10). Using this approach, Gunatilaka et al. [76] demonstrated that
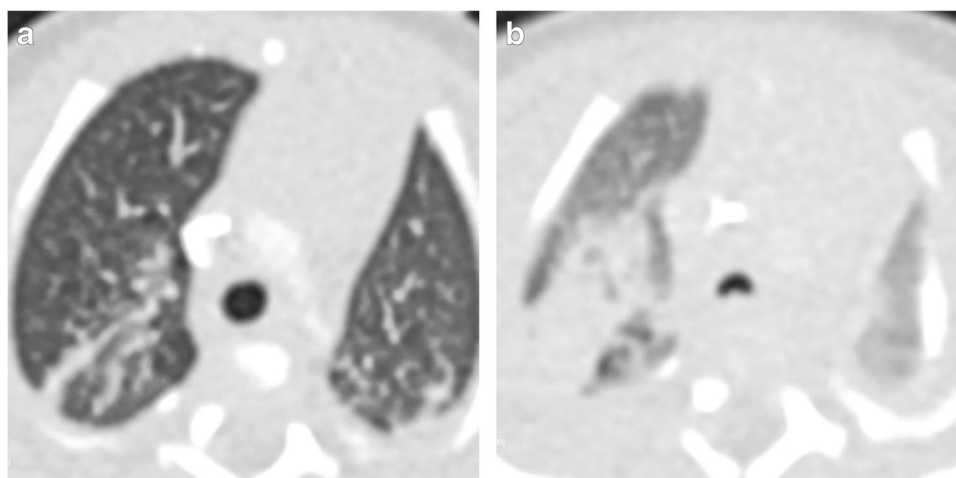
Fig. 7 Airway pressure imaging in a preterm boy born at 25 weeks of gestation, now post-menstrual age 31 weeks (6 weeks old). **a, b** Axial CT demonstrates the difference in the appearance of the lungs and trachea when imaged with 14 cm of water-positive end-expiratory pressure (PEEP) (**a**) and without PEEP (**b**). Airway pressure support is often needed but can mask tracheobronchomalacia when it is present. Removing the pressure support at the time of imaging can be very helpful in evaluating the lungs and the airway when performing CT

neonates with tracheomalacia used more than 10 times the energy to breathe that they would have with static airways.

A similar approach of imaging based computational fluid dynamics has also been used to assess the effect of subglottic stenosis on neonatal breathing, revealing that the increased airway resistance caused by the stenosis is associated not only with the degree of stenotic narrowing [104, 105] but also with the axial position of the stenosis [75].

Central airway computed tomography

As a more readily available modality, CT is much more commonly used to assess for tracheobronchomalacia and other central airway anatomies in infants with BPD, using a relatively low radiation dose, with airway abnormalities detected from scans exposing subjects to less than 2 mSv [106].

Various studies have used CT to diagnose tracheobronchomalacia in infants with and without BPD with sensitivity values ranging 75–100% (and as low as 37.5% for tracheomalacia alone) and specificity of 48–97% [107–109]. Differences in these results stem from differences in the age range of children, the use of static or dynamic CT, the phase of breathing or breathing maneuver in which imaging was acquired, and the technique used to determine the presence of tracheobronchomalacia from CT images. The change in tracheal lumen cross-sectional area at the point of greatest collapse is higher in infants with tracheobronchomalacia than in those without tracheobronchomalacia [55, 110, 111]. However, another study found CT is less sensitive than tracheobronchography in the diagnosis of tracheomalacia in ventilator-dependent infants and exposes them to a higher radiation dose [112]. In addition to the detection of tracheobronchomalacia, dynamic CT provides enough fidelity in airway measurement to be used to set ventilator-positive end-expiratory pressure settings [52].

Pulmonary vasculature and pulmonary hypertension

Bronchopulmonary dysplasia is associated with pulmonary vascular disease and pulmonary hypertension because of alterations in development of pulmonary parenchyma and vasculature [113–115]. The presence of cor pulmonale was noted by Northway et al. [10] in the autopsy specimens of five long-term survivors of preterm birth. Currently, there is a renewed interest in BPD-associated pulmonary hypertension. The incidence of BPD–pulmonary hypertension increases with severity of BPD, with 20–40% incidence of pulmonary hypertension in infants with severe BPD [95, 116]. Infants with BPD-associated pulmonary vascular disease and pulmonary hypertension have worse outcomes, including longer duration of respiratory support [95, 114, 117], increased incidence of respiratory disease in early childhood [113] and increased mortality [94, 114, 117–120] compared to infants with BPD but without pulmonary vascular disease or pulmonary hypertension. The increased morbidity and mortality associated with BPD pulmonary vascular disease and pulmonary hypertension has resulted in research focused on the early identification and diagnosis, risk stratification and pharmacological therapy for these children [3].

Fig. 8 The Myer-Cotton scale.
a–e Endoscopic images of
infants with bronchopulmonary
dysplasia (BPD) demonstrate a
normal subglottis (**a**) followed
by examples of the Myer-Cotton
subglottic stenosis grading
system. Grade 1 is defined
as < 50% obstruction (**b**), grade
2 as 51–70% obstruction (**c**),
grade 3 as 71–99% obstruction
(**d**) and grade 4 as complete
100% obstruction (**e**)
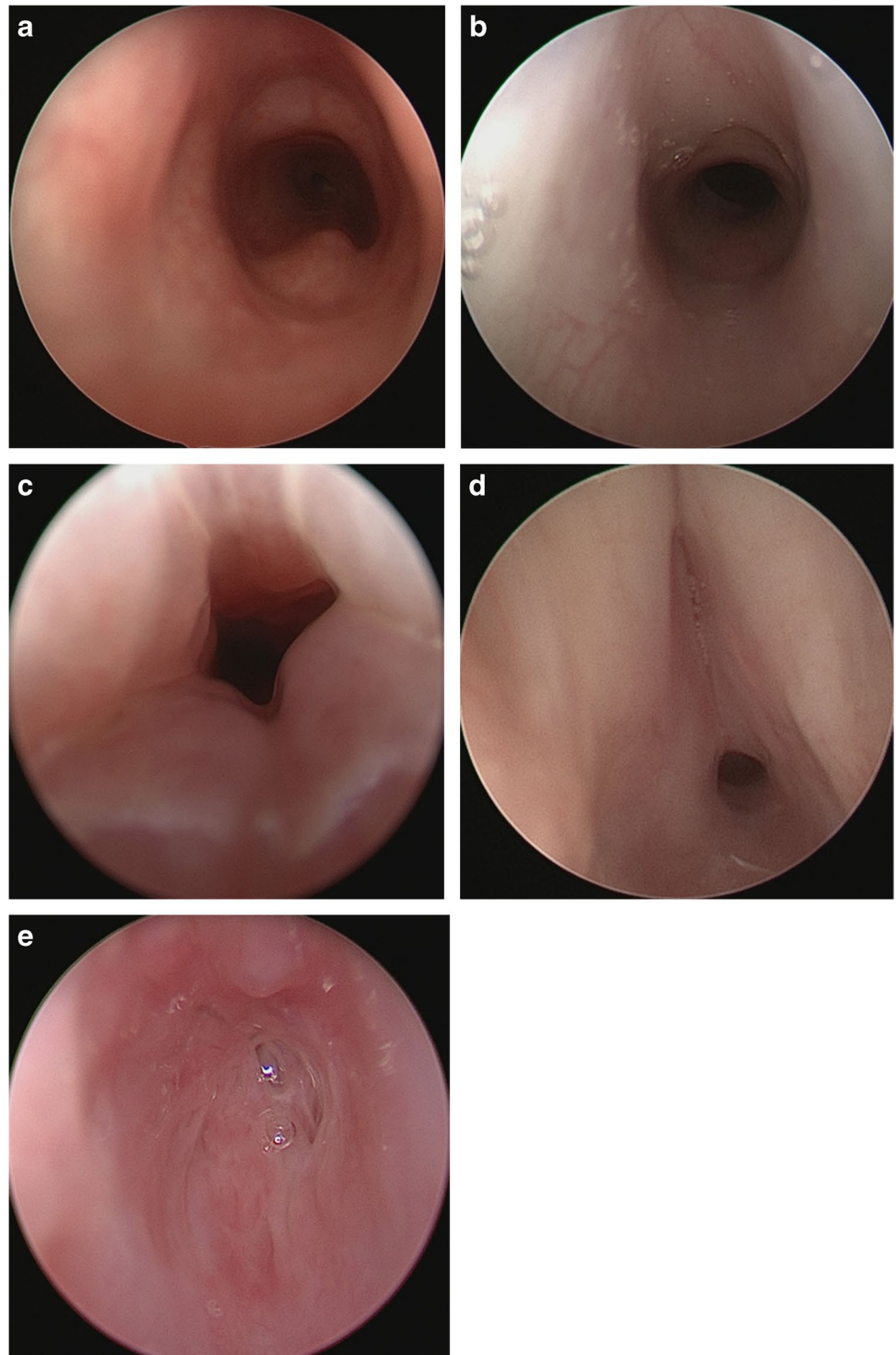
While cardiac catheterization remains the gold standard for diagnosing pulmonary hypertension [121], echocardiography is the predominant modality for screening and monitoring BPD–pulmonary hypertension. Echocardiographic evidence of pulmonary vascular disease at 7 days of age was associated with respiratory disease in early childhood [114], and current guidelines recommend screening in all infants at the time of BPD diagnosis [122]. Echocardiography evaluation of BPD-associated pulmonary hypertension should include a complete anatomical survey; assessment of right and left ventricular size, function and hypertrophy; right ventricular pressure; and presence of any anatomical shunts [122]. In particular, the presence and size of a patent ductus arteriosus is of particular importance. Evaluation

Fig. 9 Assessing the cross-sectional area of the tracheal lumen based on ultrashort echo-time (UTE) MRI in a preterm girl born at 25 weeks of gestation, now post-menstrual age 38 weeks (13 weeks old) with severe bronchopulmonary dysplasia and tracheomalacia. Bronchoscopic axial UTE MR images (*left*) and three-dimensional (3-D) surface-rendered images (*right*) show a relatively round trachea at end-inspiration (*top row*) and inward bowing of the posterior trachealis membrane on end-expiration (*bottom row*)
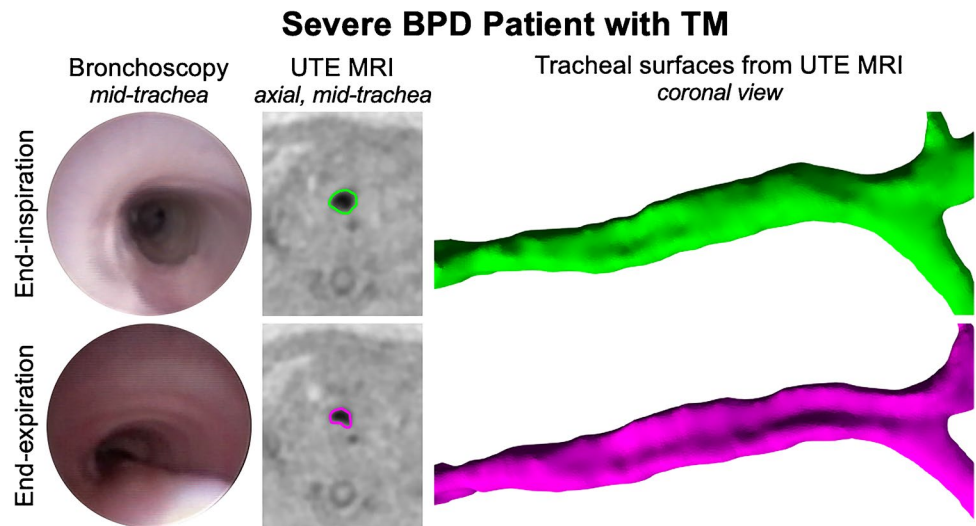
for BPD-associated pulmonary hypertension should focus on quantitative indices of right ventricular pressure including tricuspid regurgitant jet velocity, shunt gradient and left

Fig. 10 Using MRI-derived images and airflow volume, the trachea can be modeled as a non-dynamic structure (*static airway, left*) and a dynamic structure (*dynamic airway, middle*). The dynamic structure modeling results in a high-velocity jet formed in the middle of the trachea caused by narrowing during expiration, which increases work of breathing. The static airway represents the largest airway for that subject observed during breathing and represents breathing without tracheomalacia, which provides the least work of breathing. Arrows indicate the airflow direction from the main bronchi to nasopharynx. Velocity key is on the right

ventricular eccentricity index and right ventricular function, including tricuspid annular plane systolic excursion, right ventricular fractional area change, and right ventricular longitudinal strain [123]. Comprehensive echocardiographic evaluation should also include screening and evaluation of pulmonary venous return, especially presence of stenosis. Isolated or multi-vessel stenosis might be more common in the premature infant and is an independent predictor for, and an additional pathological driver of, the development of pulmonary vascular disease. It is critically important that these echocardiographic parameters be assessed in full during each echocardiographic study if possible [124, 125]. Nevertheless, assessment of these anatomical and physiological markers is often limited secondary to lung hyperinflation, cardiac malposition and poor imaging windows. Often, providers rely on qualitative markers of right ventricular hypertension (including interventricular septal flattening, which is sensitive but not specific for pulmonary hypertension and subject to interobserver variability) and qualitative assessment of right ventricular function.

Because of these limitations, additional diagnostic studies including lung perfusion scan, cardiac catheterization, chest CT or cardiac MRI should be considered when diagnostic uncertainty persists. Lung perfusion scan provides for assessment of maldistribution of pulmonary blood flow, which can result in increased pulmonary vascular resistance, and is an adjunctive diagnostic study for evaluating pulmonary vein stenosis [126]. Cardiac catheterization should be performed whenever there is concern regarding the degree of intracardiac shunting, branch pulmonary artery and pulmonary vein anatomy, left ventricular diastolic dysfunction, presence of aortopulmonary collaterals, and certainly prior to escalation of pulmonary vasodilator therapy [121]. Acute vasodilator testing is also performed during cardiac catheterization and might help guide therapy [127].
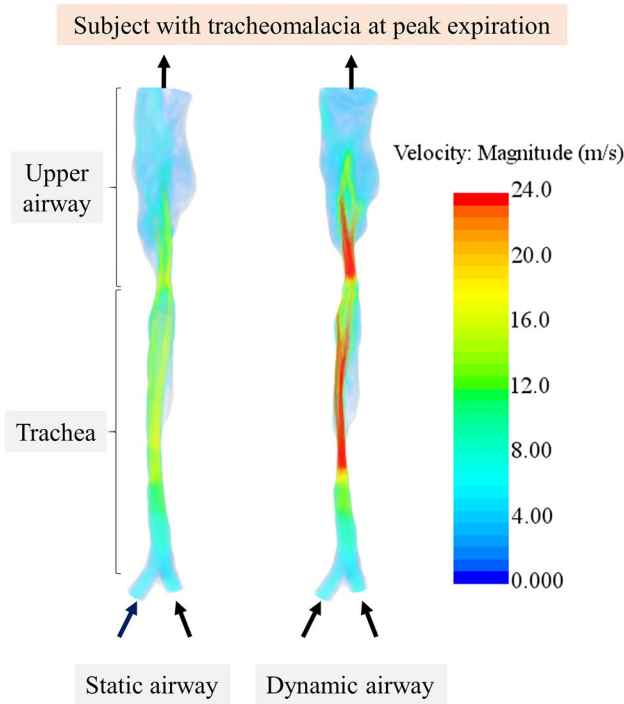
Imaging with chest CT is used in both adult and pediatric populations to assess for evidence of vascular malformations, pulmonary veno-occlusive disease, interstitial lung disease and chronic thromboembolic disease at the time of pulmonary hypertension diagnosis [121]. Additionally, chest CT has been used to assess morphological markers of pulmonary hypertension including the main pulmonary artery size and main pulmonary artery to aorta (PA/AO) ratio (Fig. 11) [128–130]. No studies have investigated the role of chest CT in the diagnosis of BPD-associated pulmonary hypertension. However, del Cerro and colleagues
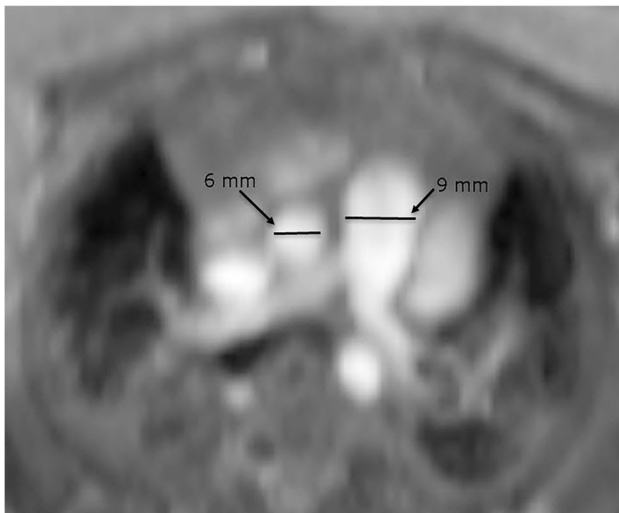

Fig. 11 Morphological markers of pulmonary hypertension in a girl born at 26 weeks of gestation with MRI performed at post-menstrual age 38 weeks (12 weeks old). Axial MRI bright-blood image through the main pulmonary artery and the ascending aorta demonstrates a 9-mm main pulmonary artery and a 6-mm aorta, resulting in a ratio of 1.5:1. A ratio of 1.3:1 or greater, in the absence of a larger left-to-right shunt, is very specific for pulmonary hypertension

[131] found that 19/29 (66%) infants with BPD-associated pulmonary hypertension had aortopulmonary collaterals, pulmonary vein stenosis, atrial septal defect or patent ductus arteriosus diagnosed with CT or catheterization. Additionally, CT was shown to aid in the diagnosis of pulmonary vein stenosis in infants with BPD in a multicenter retrospective study [124]. These data suggest that CT could have a clinical role in identifying vascular pathology or characterizing shunt lesions prior to surgical or percutaneous intervention in the BPD-associated pulmonary hypertension population.

Cardiac MRI allows for evaluation of cardiac morphology, ventricular size and function, cardiac output, and pulmonary blood flow distribution. Assessment with cardiac MRI is used in the adult and pediatric pulmonary hypertension populations where MRI-derived right ventricular function has been associated with mortality [132, 133]. In a cohort of 52 infants, the PA/AO ratio was associated with BPD severity, duration of respiratory support, hospitalization length and need for pulmonary vasodilator therapy [134]. In that study, ventricular size, ventricular function, cardiac output and pulmonary blood flow could be determined but were not associated with BPD severity or short-term clinical outcomes.

Cardiac MRI markers of right ventricular afterload have been associated with invasive hemodynamics in the pediatric pulmonary hypertension population [135, 136]. Left ventricular eccentricity index (Fig. 12), a quantitative marker of interventricular septal flattening that is typically measured at end-systole, was associated with duration of respiratory support, hospitalization length and need for pulmonary vasodilator therapy in infants with BPD [134, 137]. Further, interventricular septal curvature (Fig. 13), which provides a quantitative evaluation of septal flattening throughout the cardiac cycle, demonstrated improved discrimination of
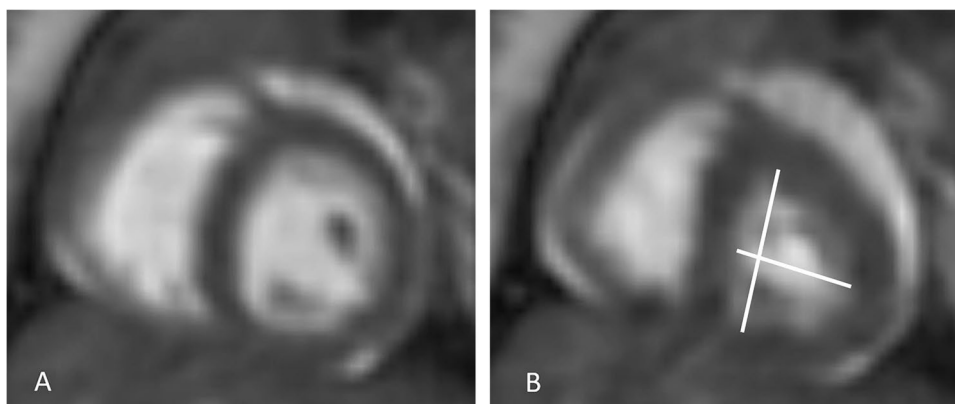

Fig. 12 Left ventricular eccentricity index in a boy born at 24 weeks of gestation and imaged at post-menstrual age 40 weeks (16 weeks old). **a, b** MRI short-axis cine steady-state free precession (SSFP) slice at the level of the papillary muscles shows diastole (**a**) and sys-

tole (**b**). During systole, the interventricular septum is clearly flattened, creating a D-shape left ventricle. A left ventricular eccentricity index greater than 1.3:1 is diagnostic of pulmonary hypertension
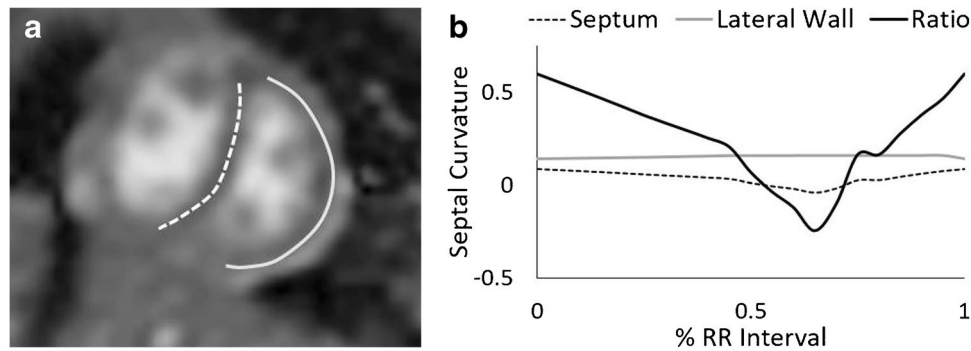
Fig. 13 Preterm male born at 24 weeks of gestation, now postmenstrual age 31 weeks (7 weeks old). **a, b** MR septal curvature is derived as the ratio of curvature of the interventricular septum (*dashed line*) and lateral wall (*solid line*) throughout the cardiac cycle (**a**). MRI short-axis cine steady-state free precession (SSFP) image shown here demonstrates the phase in the cardiac cycle at which minimum septal curvature occurred (**a**). In this case the interventricular septum is everted, resulting in a negative septal curvature value. Septal curvature throughout the cardiac cycle for the interventricular septum (*dashed line*), lateral wall (*gray line*), and ratio of the interventricular septum to the lateral wall (*black line*, **b**)

need for pulmonary vasodilator therapy compared to other clinical and cardiac MRI indices [137].

Management of BPD-associated pulmonary hypertension focuses on providing adequate respiratory support; treatment of hypoxia, infection, aspiration and airway disease; followed by treatment with pulmonary vasodilator therapy if pulmonary hypertension persists [121]. Cohen et al. [138] reported on a cohort of 269 pediatric patients treated with sildenafil, including 135 infants with BPD-associated pulmonary hypertension. Mortality in recent BPD-associated pulmonary hypertension cohorts was improved compared to historical cohorts [121, 138, 139]. Additionally, 45% of these children were able to discontinue sildenafil therapy after improvement in pulmonary hypertension. While these results are encouraging, infants with BPD-associated pulmonary hypertension remain at risk for developing pulmonary vascular disease and pulmonary hypertension later in life. Recently preterm birth, in the absence of BPD, has been associated with pulmonary vascular disease in asymptomatic children and young adults [140, 141] supporting lifelong monitoring for pulmonary vascular disease and pulmonary hypertension in this at-risk population.

Summary — putting it all together

Chronic respiratory disease of prematurity is best thought of as a disease that affects all components of the cardiopulmonary system: the lung parenchyma, small airways, large airways, pulmonary vasculature and heart. This creates the ability to "phenotype" infants based on the disease presence and severity of each component [55]. Among children with severe BPD, tracheobronchomalacia and pulmonary hypertension are also likely to be present, but a child with mild lung disease could also have tracheobronchomalacia or pulmonary hypertension. Such a child could be predicted to have a more difficult course after discharge than a preterm baby without an additional comorbidity. Therefore, knowledge of the child's phenotype from imaging is very important.

Chest radiograph is very limited in its ability to characterize all three aspects of disease — BPD, tracheobronchomalacia and pulmonary hypertension — but a bubbly cystic appearance with coarse opacities intermixed with hyperlucent areas does predict severity and is now part of the BPD definition [3]. However, it does not provide much information about the airway or cardiovascular involvement that can have such an important impact on outcomes.

On the other hand, chest CT can provide detailed evaluation of the lungs for air-trapping, cysts, mosaic perfusion and opacities, which can range from linear bands and small triangular opacities against the pleura to large confluent opacities. Additionally, on CT the trachea is well evaluated for the presence or absence of tracheobronchomalacia. There are several methods to perform the chest CT: inspiration/expiration CT, inspiration only or during tidal breathing. Several papers in the review used inspiration/expiration techniques, but that usually requires sedation or general anesthesia [5]. Our recommendation based on experience is to image during tidal breathing using either feed-and-swaddle technique or minimal sedation if needed. Temporary removal of any sort of airway pressure support reveals the true nature of the trachea and bronchi.

The addition of contrast agent to a chest CT can be considered. Advantages are that the vessels can be visualized. The PA/AO ratio could indicate the presence of pulmonary hypertension, a ductus arteriosus or other left-to-right shunt, and could even help to evaluate interventricular septal flattening. The disadvantage of giving contrast agent is the potential for infant movement during injection. Additionally,

CT angiography can be used to evaluate the pulmonary veins for stenosis. However, echocardiography remains the primary method of evaluating for pulmonary hypertension and pulmonary vein stenosis.

Magnetic resonance imaging of the lungs, heart and trachea is on the cusp of becoming a clinical reality, with UTE imaging playing a large role in providing CT-like imaging of the lung but also dynamic imaging of the trachea during tidal breathing. Imaging of the heart and vasculature can be performed without contrast agent. Thus, MRI can assess the PA/AO ratio, septal flattening and septal curvature, which is a very good measure of the severity of BPD–pulmonary hypertension [134, 137]. Evaluation of the pulmonary veins would likely require the use of contrast agent.

One of the exciting and novel uses of the dynamic UTE images of the lung is the ability to use the signal intensity over the respiratory cycle to determine regional ventilation [77]. A similar process could be done with dynamic CT data, but only over one or two breathing cycles. The advantage of the MRI is a much higher temporal resolution and a single composite breathing cycle created from several minutes of imaging and the absence of radiation [65].

Radiologists have always played a significant role in the care and treatment of preterm babies via a variety of imaging modalities. Imaging of the pulmonary system likely has played the greatest role for radiology and now there is new evidence that cross-sectional imaging has added value in characterizing the contributions of the lung, large airways and cardiovascular system to the child's clinical status and in predicting morbidity.

Declarations

Conflicts of interest None

References

1. World Health Organization (2018) Preterm birth: key facts. http://www.who.int/news-room/fact-sheets/detail/preterm-birth. Accessed 28 Feb 2021

2. Centers for Disease Control and Prevention (2020) Reproductive health: premature birth. http://www.cdc.gov/reproductivehealth/features/premature-birth. Accessed 28 Feb 2021

3. Higgins RD, Jobe AH, Koso-Thomas M et al (2018) Bronchopulmonary dysplasia: executive summary of a workshop. J Pediatr 197:300–308

4. Bonadies L, Zaramella P, Porzionato A et al (2020) Present and future of bronchopulmonary dysplasia. J Clin Med 9:1539

5. Sung T, Hwang SM, Kim MY et al (2018) Relationship between clinical severity of "new" bronchopulmonary dysplasia and HRCT abnormalities in VLBW infants. Pediatr Pulmonol 53:1391–1398

6. Shepherd EG, Luca D (2020) New imaging tools allow bronchopulmonary dysplasia to enter the age of precision medicine. Am J Respir Crit Care Med 202:924–926

7. Wildman-Tobriner B, Strauss KJ, Bhargavan-Chatfield M et al (2018) Using the American College of Radiology dose index registry to evaluate practice patterns and radiation dose estimates of pediatric body CT. AJR Am J Roentgenol 210:641–647

8. Higano NS, Spielberg DR, Fleck RJ et al (2018) Neonatal pulmonary magnetic resonance imaging of bronchopulmonary dysplasia predicts short-term clinical outcomes. Am J Respir Crit Care Med 198:1302–1311

9. Hahn AD, Higano NS, Walkup LL et al (2016) Pulmonary MRI of neonates in the intensive care unit using 3D ultrashort echo time and a small footprint MRI system. J Magn Reson Imaging 45:463–471

10. Northway WH, Rosan RC, Porter DY (1967) Pulmonary disease following respiratory therapy of hyaline-membrane disease — bronchopulmonary dysplasia. New Engl J Med 276:357–368

11. Day CL, Ryan RM (2017) Bronchopulmonary dysplasia: new becomes old again! Pediatr Res 81:210–213

12. Shennan A, Dunn M, Ohlsson A et al (1988) Abnormal pulmonary outcomes in premature infants: prediction from oxygen requirement in the neonatal period. Pediatrics 82:527–532

13. Jobe AH, Bancalari E (2012) Bronchopulmonary dysplasia. Am J Resp Crit Care Med 163:1723–1729

14. Walsh MC, Wilson-Costello D, Zadell A et al (2003) Safety, reliability, and validity of a physiologic definition of bronchopulmonary dysplasia. J Perinatol 23:451–456

15. Isayama T, Lee SK, Yang J et al (2017) Revisiting the definition of bronchopulmonary dysplasia: effect of changing panoply of respiratory support for preterm neonates. JAMA Pediatr 171:271–279

16. Poindexter BB, Feng R, Schmidt B et al (2015) Comparisons and limitations of current definitions of bronchopulmonary dysplasia for the prematurity and respiratory outcomes program. Ann Am Thorac Soc 12:1822–1830

17. Thunqvist P, Gustafsson P, Norman M et al (2015) Lung function at 6 and 18 months after preterm birth in relation to severity of bronchopulmonary dysplasia. Pediatr Pulmonol 50:978–986

18. Sanchez-Solis M, Garcia-Marcos L, Bosch-Gimenez V et al (2012) Lung function among infants born preterm, with or without bronchopulmonary dysplasia. Pediatr Pulmonol 47:674–681

19. Morrow LA, Wagner BD, Ingram DA et al (2017) Antenatal determinants of bronchopulmonary dysplasia and late respiratory disease in preterm infants. Am J Respir Crit Care Med 196:364–374

20. Bancalari E, Abdenour GE, Feller R, Gannon J (1979) Bronchopulmonary dysplasia: clinical presentation. J Pediatr 95:819–823

21. Toce SS, Farrell PM, Leavitt LA et al (1984) Clinical and roentgenographic scoring systems for assessing bronchopulmonary dysplasia. Am J Dis Child 138:581–585

22. Polin RA, Carlo WA, Committee on Fetus and Newborn, American Academy of Pediatrics (2014) Surfactant replacement therapy for preterm and term neonates with respiratory distress. Pediatrics 133:156–163

23. Halliday HL (2017) The fascinating story of surfactant. J Paediatr Child Health 53:327–332

24. Swischuk LE, Shetty BP, John SD (1996) The lungs in immature infants: how important is surfactant therapy in preventing chronic lung problems? Pediatr Radiol 26:508–511

25. Breysem L, Smet M-H, Lierde SV et al (1997) Bronchopulmonary dysplasia: correlation of radiographic and clinical findings. Pediatr Radiol 27:642–646

26. May C, Prendergast M, Salman S et al (2009) Chest radiograph thoracic areas and lung volumes in infants developing bronchopulmonary dysplasia. Pediatr Pulmonol 44:80–85

27. Dassios T, Curley A, Krokidis M et al (2016) Correlation of radiographic thoracic area and oxygenation impairment in bronchopulmonary dysplasia. Respir Physiol Neurobiol 220:40–45

28. Moya MP, Bisset GS 3rd, Auten RL Jr et al (2001) Reliability of CXR for the diagnosis of bronchopulmonary dysplasia. Pediatr Radiol 31:339–342

29. Kim H, Kim JY, Yun BL et al (2017) Interstitial pneumonia pattern on day 7 chest radiograph predicts bronchopulmonary dysplasia in preterm infants. BMC Pediatr 17:125

30. Hyödynmaa E, Korhonen P, Ahonen S et al (2012) Frequency and clinical correlates of radiographic patterns of bronchopulmonary dysplasia in very low birth weight infants by term age. Eur J Pediatr 171:95–102

31. Arai H, Ito M, Ito T et al (2020) Bubbly and cystic appearance on chest radiograph of extremely preterm infants with bronchopulmonary dysplasia is associated with wheezing disorder. Acta Paediatr 109:711–719

32. Arai H, Ito T, Ito M et al (2019) Impact of chest radiography-based definition of bronchopulmonary dysplasia. Pediatr Int 61:258–263

33. Luo H, Wang L, Chen P et al (2019) Neonatal respiratory status predicts longitudinal respiratory health outcomes in preterm infants. Pediatr Pulmonol 54:814–821

34. Howling SJ, Northway WH, Hansell DM et al (2000) Pulmonary sequelae of bronchopulmonary dysplasia survivors: high-resolution CT findings. AJR Am J Roentgenol 174:1323–1326

35. Kubota J, Ohki Y, Inoue T et al (1998) Ultrafast CT scoring system for assessing bronchopulmonary dysplasia: reproducibility and clinical correlation. Radiat Med 16:167–164

36. Aquino SL, Schechter MS, Chiles C et al (1999) High-resolution inspiratory and expiratory CT in older children and adults with bronchopulmonary dysplasia. AJR Am J Roentgenol 173:963–967

37. Aukland SM, Rosendahl K, Owens CM et al (2009) Neonatal bronchopulmonary dysplasia predicts abnormal pulmonary HRCT scans in long-term survivors of extreme preterm birth. Thorax 64:405

38. Aukland SM, Halvorsen T, Fosse KR et al (2006) High-resolution CT of the chest in children and young adults who were born prematurely: findings in a population-based study. AJR Am J Roentgenol 187:1012–1018

39. Mahut B, De Blic J, Emond S et al (2007) Chest computed tomography findings in bronchopulmonary dysplasia and correlation with lung function. Arch Dis Child Fetal Neonatal Ed 92:F459

40. Ochiai M, Hikino S, Yabuuchi H et al (2008) A new scoring system for computed tomography of the chest for assessing the clinical status of bronchopulmonary dysplasia. J Pediatr 152:90–95.e3

41. Bastos Boechat MC, Reis de Mello R, Silveira da Silva K et al (2010) A computed tomography scoring system to assess pulmonary disease among premature infants. Sao Paulo Med J 128:328–335

42. Caskey S, Gough A, Rowan S et al (2016) Structural and functional lung impairment in adult survivors of bronchopulmonary dysplasia. Ann Am Thorac Soc 13:1262–1270

43. Ronkainen E, Perhomaa M, Mattila L et al (2018) Structural pulmonary abnormalities still evident in schoolchildren with new bronchopulmonary dysplasia. Neonatology 113:122–130

44. Tonson la Tour A, Spadola L, Sayegh Y et al (2013) Chest CT in bronchopulmonary dysplasia: clinical and radiological correlations. Pediatr Pulmonol 48:693–698

45. Sarria EE, Mattiello R, Rao L et al (2011) Computed tomography score and pulmonary function in infants with chronic lung disease of infancy. Eur Respir J 38:918–923

46. Sarria EE, Mattiello R, Rao L et al (2011) Quantitative assessment of chronic lung disease of infancy using computed tomography. Eur Respir J 39:992–999

47. Simpson SJ, Logie KM, O'Dea CA et al (2017) Altered lung structure and function in mid-childhood survivors of very preterm birth. Thorax 72:702

48. Simpson SJ, Turkovic L, Wilson AC et al (2018) Lung function trajectories throughout childhood in survivors of very preterm birth: a longitudinal cohort study. Lancet Child Adolesc Health 2:350–359

49. Spielberg DR, Walkup LL, Stein JM et al (2018) Quantitative CT scans of lung parenchymal pathology in premature infants ages 0–6 years. Pediatr Pulmonol 53:316–323

50. Shin S-M, Kim WS, Cheon J-E et al (2012) Bronchopulmonary dysplasia: new high resolution computed tomography scoring system and correlation between the high resolution computed tomography score and clinical severity. Korean J Radiol 14:350–360

51. van Mastrigt E, Logie K, Ciet P et al (2016) Lung CT imaging in patients with bronchopulmonary dysplasia: a systematic review. Pediatr Pulmonol 51:975–986

52. May LA, Jadhav SP, Guillerman RP et al (2019) A novel approach using volumetric dynamic airway computed tomography to determine positive end-expiratory pressure (PEEP) settings to maintain airway patency in ventilated infants with bronchopulmonary dysplasia. Pediatr Radiol 49:1276–1284

53. Hysinger EB, Friedman NL, Padula MA et al (2017) Tracheobronchomalacia is associated with increased morbidity in bronchopulmonary dysplasia. Ann Am Thorac Soc 14:1428–1435

54. Pennati F, Salito C, Roach D et al (2015) Regional ventilation in infants quantified by multi-volume high resolution computed tomography (HRCT) and multi-volume proton magnetic resonance imaging (MRI). Eur Respir J 46:OA2949

55. Wu KY, Jensen EA, White AM et al (2019) Characterization of disease phenotype in very preterm infants with severe bronchopulmonary dysplasia. Am J Respir Crit Care Med 201:1398–1406

56. Walkup LL, Tkach JA, Higano NS et al (2015) Quantitative magnetic resonance imaging of bronchopulmonary dysplasia in the neonatal intensive care unit environment. Am J Respir Crit Care Med 192:1215–1222

57. Schopper MA, Walkup LL, Tkach JA et al (2017) Evaluation of neonatal lung volume growth by pulmonary magnetic resonance imaging in patients with congenital diaphragmatic hernia. J Pediatrics 188:96–102.e1

58. Hatabu H, Ohno Y, Gefter WB et al (2020) Expanding applications of pulmonary MRI in the clinical evaluation of lung disorders: Fleischner Society position paper. Radiology 297:286–301

59. Johnson KM, Fain SB, Schiebler ML, Nagle S (2013) Optimized 3D ultrashort echo time pulmonary MRI. Magn Reson Med 70:1241–1250

60. Lederlin M, Crémillieux Y (2014) Three-dimensional assessment of lung tissue density using a clinical ultrashort echo time at 3 tesla: a feasibility study in healthy subjects. J Magn Reson Imaging 40:839–847

61. Dournes G, Grodzki D, Macey J et al (2015) Quiet submillimeter MR imaging of the lung is feasible with a PETRA sequence at 1.5 T. Radiology 276:258–265

62. Roach DJ, Ruangnapa K, Fleck RJ et al (2019) Structural lung abnormalities on computed tomography correlate with asthma inflammation in bronchoscopic alveolar lavage fluid. J Asthma 57:968–979

63. Willmering MM, Robison RK, Wang H et al (2019) Implementation of the FLORET UTE sequence for lung imaging. Magn Reson Med 82:1091–1100

64. Nozawa K, Niwa T, Aida N (2019) Imaging of cystic lung lesions in infants using pointwise encoding time reduction with radial acquisition (PETRA). Magn Reson Med Sci 18:299–300

65. Higano NS, Fleck RJ, Spielberg DR et al (2017) Quantification of neonatal lung parenchymal density via ultrashort echo time MRI with comparison to CT. J Magn Reson Imaging 46:992–1000

66. Higano N, Fleck R, Schapiro A et al (2020) Lung MRI in neonatal bronchopulmonary dysplasia: objective quantification of lung density abnormalities correlates with short-term respiratory outcomes. Am J Respir Crit Car Med 201:A5973

67. Weick S, Breuer FA, Ehses P et al (2013) DC-gated high resolution three-dimensional lung imaging during free-breathing. J Magn Reson Imaging 37:727–732

68. Richter JAJ, Wech T, Weng AM et al (2020) Free-breathing self-gated 4D lung MRI using wave-CAIPI. Magn Reson Med 84:3223–3233

69. Higano NS, Hahn AD, Tkach JA et al (2017) Retrospective respiratory self-gating and removal of bulk motion in pulmonary UTE MRI of neonates and adults. Magn Reson Med 77:1284–1295

70. Jiang W, Ong F, Johnson KM et al (2018) Motion robust high resolution 3D free-breathing pulmonary MRI using dynamic 3D image self-navigator. Magn Reson Med 79:2954–2967

71. Tibiletti M, Bianchi A, Kjørstad Å et al (2017) Respiratory self-gated 3D UTE for lung imaging in small animal MRI. Magn Reson Med 78:739–745

72. Zhu X, Chan M, Lustig M et al (2020) Iterative motion-compensation reconstruction ultra-short TE (iMoCo UTE) for high-resolution free-breathing pulmonary MRI. Magn Reson Med 83:1208–1221

73. Yoder LM, Higano NS, Schapiro AH et al (2019) Elevated lung volumes in neonates with bronchopulmonary dysplasia measured via MRI. Pediatr Pulmonol 54:1311–1318

74. Bates AJ, Higano NS, Hysinger EB et al (2019) Quantitative assessment of regional dynamic airway collapse in neonates via retrospectively respiratory-gated 1H ultrashort echo time MRI. J Magn Reson Imaging 49:659–667

75. Hysinger EB, Bates AJ, Higano NS et al (2020) Ultrashort echo-time MRI for the assessment of tracheomalacia in neonates. Chest 157:595–602

76. Gunatilaka CC, Higano NS, Hysinger EB et al (2020) Increased work of breathing due to tracheomalacia in neonates. Ann Am Thorac Soc 17:1247–1256

77. Guerrero T, Sanders K, Noyola-Martinez J et al (2005) Quantification of regional ventilation from treatment planning CT. Int J Radiat Oncol Biol Phys 62:630–634

78. Capaldi DPI, Guo F, Xing L, Parraga G (2020) Pulmonary ventilation maps generated with free-breathing proton MRI and a deep convolutional neural network. Radiology 298:427–438

79. Lutey BA, Lefrak SS, Woods JC et al (2008) Hyperpolarized ^{3}He MR imaging: physiologic monitoring observations and safety considerations in 100 consecutive subjects. Radiology 248:655–661

80. Driehuys B, Martinez-Jimenez S, Cleveland ZI et al (2012) Chronic obstructive pulmonary disease: safety and tolerability of hyperpolarized ^{129}Xe MR imaging in healthy volunteers and patients. Radiology 262:279–289

81. Walkup LL, Thomen RP, Akinyi TG et al (2016) Feasibility, tolerability and safety of pediatric hyperpolarized ^{129}Xe magnetic resonance imaging in healthy volunteers and children with cystic fibrosis. Pediatr Radiol 46:1651–1662

82. Fain SB, Panth SR, Evans MD et al (2006) Early emphysematous changes in asymptomatic smokers: detection with ^{3}He MR imaging. Radiology 239:875–883

83. Thomen RP, Walkup LL, Roach DJ et al (2020) Regional structure-function in cystic fibrosis lung disease using hyperpolarized ^{129}Xe and ultrashort echo magnetic resonance imaging. Am J Respir Crit Care Med 202:290–292

84. Cadman RV, Lemanske RF, Evans MD et al (2013) Pulmonary ^{3}He magnetic resonance imaging of childhood asthma. J Allergy Clin Immunol 131(369–376):e1–5

85. Altes TA, Meyer CH, Mata JF et al (2017) Hyperpolarized helium-3 magnetic resonance lung imaging of non-sedated infants and young children: a proof-of-concept study. Clin Imaging 45:105–110

86. Woods JC, Choong CK, Yablonskiy DA et al (2006) Hyperpolarized ^{3}He diffusion MRI and histology in pulmonary emphysema. Magn Reson Med 56:1293–1300

87. Flors L, Mugler JP, Paget-Brown A et al (2017) Hyperpolarized helium-3 diffusion-weighted magnetic resonance imaging detects abnormalities of lung structure in children with bronchopulmonary dysplasia. J Thorac Imaging 32:323–332

88. Higano NS, Thomen RP, Quirk JD et al (2021) Alveolar airspace size in healthy and diseased infant lungs measured via hyperpolarized ^{3}He gas diffusion magnetic resonance imaging. Neonatology 117:704–712

89. Deoras KS, Wolfson MR, Searls RL et al (1991) Developmental changes in tracheal structure. Pediatr Res 30:170–175

90. Deoras KS, Wolfson MR, Bhutani VK, Shaffer TH (1989) Structural changes in the tracheae of preterm lambs induced by ventilation. Pediatr Res 26:434–437

91. Croteau JR, Cook CD (1961) Volume-pressure and length-tension measurements in human tracheal and bronchial segments. J Appl Physiol 16:170–172

92. Bhutani VK, Shaffer TH (1982) Time-dependent tracheal deformation in fetal, neonatal, and adult rabbits. Pediatr Res 16:830–833

93. Cohn RC, Kercsmar C, Dearborn D (1988) Safety and efficacy of flexible endoscopy in children with bronchopulmonary dysplasia. Am J Dis Child 142:1225–1228

94. Wallis C, Alexopoulou E, Antón-Pacheco JL et al (2019) ERS statement on tracheomalacia and bronchomalacia in children. Eur Respir J 54:1900382

95. Lagatta JM, Hysinger EB, Zaniletti I et al (2018) The impact of pulmonary hypertension in preterm infants with severe bronchopulmonary dysplasia through 1 year. J Pediatrics 203:218–224.e3

96. Walner DL, Loewen MS, Kimura RE (2001) Neonatal subglottic stenosis — incidence and trends. Laryngoscope 111:48–51

97. Thomas RE, Rao SC, Minutillo C et al (2018) Severe acquired subglottic stenosis in neonatal intensive care graduates:

a case–control study. Arch Dis Child Fetal Neonatal Ed 103:F349–F354

98. Myer CM, O'Connor DM, Cotton RT (1994) Proposed grading system for subglottic stenosis based on endotracheal tube sizes. Ann Otol Rhinol Laryngol 103:319–323

99. Lang M, Brietzke SE (2013) A systematic review and meta-analysis of endoscopic balloon dilation of pediatric subglottic stenosis. Otolaryngol Head Neck Surg 150:174–179

100. Maresh A, Preciado DA, O'Connell AP, Zalzal GH (2014) A comparative analysis of open surgery vs endoscopic balloon dilation for pediatric subglottic stenosis. JAMA Otolaryngol Head Neck Surg 140:901–905

101. Faust RA, Rimell FL, Remley KB (2002) Cine magnetic resonance imaging for evaluation of focal tracheomalacia: innominate artery compression syndrome. Int J Pediatr Otorhinolaryngol 65:27–33

102. Faust RA, Remley KB, Rimell FL (2001) Real-time, cine magnetic resonance imaging for evaluation of the pediatric airway. Laryngoscope 111:2187–2190

103. Gandhi DB, Rice A, Gunatilaka CC et al (2021) Quantitative evaluation of subglottic stenosis using ultrashort echo time MRI in a rabbit model. Laryngoscope 131:E1971–E1979

104. Poynot WJ, Gonthier KA, Dunham ME, Crosby TW (2020) Classification of tracheal stenosis in children based on computational aerodynamics. J Biomech 104:109752

105. Lin EL, Bock JM, Zdanski CJ et al (2018) Relationship between degree of obstruction and airflow limitation in subglottic stenosis. Laryngoscope 128:1551–1557

106. Greenberg SB (2012) Dynamic pulmonary CT of children. AJR Am J Roentgenol 199:435–440

107. Lee S, Im SA, Yoon J (2014) Tracheobronchomalacia in infants: the use of non-breath held 3D CT bronchoscopy. Pediatr Pulmonol 49:1028–1035

108. Tan JZ, Crossett M, Ditchfield M (2013) Dynamic volumetric computed tomographic assessment of the young paediatric airway: initial experience of rapid, non-invasive, four-dimensional technique. J Med Imaging Radiat Oncol 57:141–148

109. Ullmann N, Secinaro A, Menchini L et al (2018) Dynamic expiratory CT: an effective non-invasive diagnostic exam for fragile children with suspected tracheo-bronchomalacia. Pediatr Pulmonol 53:73–80

110. Douros K, Kremmydas G, Grammeniatis V et al (2019) Helical multi-detector CT scan as a tool for diagnosing tracheomalacia in children. Pediatr Pulmonol 54:47–52

111. Goo HW (2013) Free-breathing cine CT for the diagnosis of tracheomalacia in young children. Pediatr Radiol 43:922–928

112. Mok Q, Negus S, McLaren CA et al (2005) Computed tomography versus bronchography in the diagnosis and management of tracheobronchomalacia in ventilator dependent infants. Arch Dis Child Fetal Neonatal Ed 90:F290

113. Mourani PM, Mandell EW, Meier M et al (2018) Early pulmonary vascular disease in preterm infants is associated with late respiratory outcomes in childhood. Am J Respir Crit Care Med 199:1020–1027

114. Mourani PM, Sontag MK, Younoszai A et al (2015) Early pulmonary vascular disease in preterm infants at risk for bronchopulmonary dysplasia. Am J Respir Crit Care Med 191:87–95

115. Goss KN, Everett AD, Mourani PM et al (2017) Addressing the challenges of phenotyping pediatric pulmonary vascular disease. Pulm Circ 7:7–19

116. Arjaans S, Zwart EAH, Ploegstra M et al (2018) Identification of gaps in the current knowledge on pulmonary hypertension in extremely preterm infants: a systematic review and meta-analysis. Paediatr Perinat Epidemiol 32:258–267

117. An HS, Bae EJ, Kim GB et al (2010) Pulmonary hypertension in preterm infants with bronchopulmonary dysplasia. Korean Circ J 40:131–136

118. Bhat R, Salas AA, Foster C et al (2012) Prospective analysis of pulmonary hypertension in extremely low birth weight infants. Pediatrics 129:e682–e689

119. Khemani E, McElhinney DB, Rhein L et al (2007) Pulmonary artery hypertension in formerly premature infants with bronchopulmonary dysplasia: clinical features and outcomes in the surfactant era. Pediatrics 120:1260–1269

120. Mirza H, Ziegler J, Ford S et al (2014) Pulmonary hypertension in preterm infants: prevalence and association with bronchopulmonary dysplasia. J Pediatrics 165:909–914.e1

121. Abman SH, Hansmann G, Archer SL et al (2015) Pediatric pulmonary hypertension. Circulation 132:2037–2099

122. Krishnan U, Feinstein JA, Adatia I et al (2017) Evaluation and management of pulmonary hypertension in children with bronchopulmonary dysplasia. J Pediatrics 188:24–34.e1

123. Levy PT, Jain A, Nawaytou H et al (2020) Risk assessment and monitoring of chronic pulmonary hypertension in premature infants. J Pediatrics 217:199–209.e4

124. Mahgoub L, Kaddoura T, Kameny AR et al (2017) Pulmonary vein stenosis of ex-premature infants with pulmonary hypertension and bronchopulmonary dysplasia, epidemiology, and survival from a multicenter cohort. Pediatr Pulmonol 52:1063–1070

125. Swier N, Richards B, Cua C et al (2016) Pulmonary vein stenosis in neonates with severe bronchopulmonary dysplasia. Am J Perinatol 33:671–677

126. Frank DB, Levy PT, Stiver CA et al (2021) Primary pulmonary vein stenosis during infancy: state of the art review. J Perinatol 41:1528–1539

127. Frank BS, Schäfer M, Grenolds A et al (2019) Acute vasoreactivity testing during cardiac catheterization of neonates with bronchopulmonary dysplasia-associated pulmonary hypertension. J Pediatrics 208:127–133

128. Compton GL, Florence J, MacDonald C et al (2015) Main pulmonary artery–to–ascending aorta diameter ratio in healthy children on MDCT. AJR Am J Roentgenol 205:1322–1325

129. Caro-Domínguez P, Compton G, Humpl T, Manson DE (2016) Pulmonary arterial hypertension in children: diagnosis using ratio of main pulmonary artery to ascending aorta diameter as determined by multi-detector computed tomography. Pediatr Radiol 46:1378–1383

130. Chen S-J, Huang J-H, Lee W-J et al (2019) Diagnosis of pulmonary arterial hypertension in children by using cardiac computed tomography. Korean J Radiol 20:976

131. del Cerro MJ, Rotés AS, Cartón A et al (2014) Pulmonary hypertension in bronchopulmonary dysplasia: clinical findings, cardiovascular anomalies and outcomes. Pediatr Pulmonol 49:49–59

132. van de Veerdonk MC, Kind T, Marcus JT et al (2011) Progressive right ventricular dysfunction in patients with pulmonary arterial hypertension responding to therapy. J Am Coll Cardiol 58:2511–2519

133. Moledina S, Pandya B, Bartsota M et al (2013) Prognostic significance of cardiac magnetic resonance imaging in children with pulmonary hypertension. Circ Cardiovasc Imaging 6:407–414

134. Critser PJ, Higano NS, Tkach JA et al (2019) Cardiac magnetic resonance imaging evaluation of neonatal bronchopulmonary dysplasia–associated pulmonary hypertension. Am J Respir Crit Care Med 201:73–82

135. Pandya B, Quail MA, Steeden JA et al (2018) Real-time magnetic resonance assessment of septal curvature accurately tracks acute hemodynamic changes in pediatric pulmonary hypertension. Circ Cardiovasc Imaging 7:706–713

136. Burkett DA, Patel SS, Mertens L et al (2020) Relationship between left ventricular geometry and invasive hemodynamics

in pediatric pulmonary hypertension. Circ Cardiovasc Imaging 13:e009825

137. Critser PJ, Higano NS, Lang SM et al (2020) Cardiovascular magnetic resonance imaging derived septal curvature in neonates with bronchopulmonary dysplasia associated pulmonary hypertension. J Cardiovasc Magn Reson 22:50

138. Cohen JL, Nees SN, Valencia GA et al (2019) Sildenafil use in children with pulmonary hypertension. J Pediatrics 205:29–34.e1

139. Altit G, Bhombal S, Hopper RK et al (2019) Death or resolution: the "natural history" of pulmonary hypertension in bronchopulmonary dysplasia. J Perinatol 39:415–425

140. Levy PT, Patel MD, Choudhry S et al (2018) Evidence of echocardiographic markers of pulmonary vascular disease in asymptomatic infants born preterm at one year of age. J Pediatrics 197:48–56.e2

141. Goss KN, Beshish AG, Barton GP et al (2018) Early pulmonary vascular disease in young adults born preterm. Am J Respir Crit Care Med 198:1549–1558

Publisher's note Springer Nature remains neutral with regard to jurisdictional claims in published maps and institutional affiliations.